Anomalous climate dynamics induced by multiplicative and additive noises

Dmitri V. Alexandrov ◉, Irina A. Bashkirtseva, and Lev B. Ryashko

*Department of Theoretical and Mathematical Physics, Laboratory of Multi-Scale Mathematical Modeling, Ural Federal University,
Ekaterinburg, 620000, Russian Federation*

Anomalous behavior of a nonlinear climate-vegetation model governed by the multiplicative and additive noises is revealed on the basis of stochastic sensitivity analysis. A specific feature of this model is the bistability with the coexistence of "snowball" equilibrium and "warm" attractor in the form of equilibrium or cycle. It is found that multiplicative and additive noises shift probabilistic distribution in opposite directions. The multiplicative noise introduced into the death rate of vegetation changes the dispersion of random states and their localization in the phase diagram. This type of noise cools down the system and is responsible for its transition to the snowball state. On the contrary, the additive noise warms up the climate with increasing noise intensity. A cumulative effect of multiplicative and additive noises occurs under their simultaneous influence. This effect determining the evolutionary behavior of a climate-vegetation system depends on the ratio of intensities of these noises.

I. INTRODUCTION

It is well known that the vegetation of the Earth is an indicator of climatic processes and gives a visual representation of the ongoing changes [1–3]. On the other hand, vegetative variations themselves have a major impact on climate change [4,5]. There are a large number of experimental data indicating these interactions (desertification and deforestation experiments [6–9], for example). Also, it is significant to note that these interactions can be influenced by external factors such as atmospheric CO_2 concentration, global average temperature, precipitation, or variety of vegetation. These factors, in turn, can lead to a large diversity of evolutionary scenarios of climate change [10–14]. In terms of nonlinear dynamics, this is described by different deterministic and stochastic models containing only several prognostic variables, where other variables are modeled by means of system coefficients. Therefore, to take into account the possible variability of other physical processes, we need to consider parametric and additive noises showing the variability of dynamical scenarios. As this takes place, the number of diverse evolutionary regimes increases and their full analysis requires consideration of a huge number of phase portraits and bifurcation diagrams within each climate-vegetation model. Therefore, to conduct a complete parametric analysis of the system in practice, as a rule, is not possible and the way out of this situation is the establishment of new evolutionary scenarios in the presence of stochastic forcing, as well as the determination of new effects caused by noise. As known, random forcing in nonlinear systems can cause significant changes in dynamical regimes and generate a wide variety of stochastic phenomena (see, e.g., [15–23]).

This article is concerned with the effect of multiplicative and additive noises introduced in a simple two-dimensional climate-vegetation model. This effect is caused by nonlinear interaction between two different noises that act in opposite directions and throw the climate-vegetation system to different (cold and warm) states.

This article is organized as follows. The deterministic model, as well as the corresponding bifurcation and phase diagrams, are given in Sec. II. A stochastic model is presented in Sec. III in the presence of multiplicative and additive noises. The effects of weak noise are analyzed in Sec. III A on the basis of the stochastic sensitivity technique. How the multiplicative and additive noises affect the system dynamics is respectively discussed in Secs. III B and III C. Their cumulative effect is given in Sec. III D. The main outcomes of our analysis are summarized in Sec. IV.

II. DETERMINISTIC MODEL

Let us first consider the climate-vegetation model derived by Rombouts and Ghil [24], which contains two prognostic variables: the global average temperature T and the fraction of land A covered by vegetation

$$C_T \frac{dT}{dt} = [1 - \alpha(T, A)]Q_0 - R_o(T),$$
$$\frac{dA}{dt} = \beta(T)A(1 - A) - \gamma A. \tag{1}$$

Here, C_T and Q_0 represent the heat capacity and the incoming solar energy. The total surface albedo $\alpha(T, A)$ represents three contributions connected with the ground albedo α_g, the vegetation albedo $\alpha_v < \alpha_g$, and the ocean albedo α_o. Thus, the total surface albedo reads as

$$\alpha(T, A) = p[\alpha_v A + \alpha_g(1 - A)] + (1 - p)\alpha_o(T),$$

where p and $1 - p$ are the fractions of land and ocean. In addition, the last contribution to the total albedo can be represented as [24–26]

$$\alpha_o(T) = \begin{cases} \alpha_{\max}, & T \leqslant T_{\alpha,l} \\ \alpha_{\max} + \frac{(\alpha_{\min} - \alpha_{\max})(T - T_{\alpha,l})}{T_{\alpha,u} - T_{\alpha,l}}, & T_{\alpha,l} < T \leqslant T_{\alpha,u} \\ \alpha_{\min}, & T > T_{\alpha,u} \end{cases}$$

TABLE I. Parameters used in calculations [24].

Symbol	Value	Units
C_T	500	W yr K^{-1} m^{-2}
Q_0	342.5	W m^{-2}
$T_{\alpha,l}$	263	K
$T_{\alpha,u}$	300	K
T_{opt}	283	K
B_0	200	W m^{-2}
B_1	2.5	W K^{-1} m^{-2}
k	0.004	yr^{-1} K^{-2}
p	0.3	
$\alpha_{\max}$	0.85	
$\alpha_{\min}$	0.25	
α_v	0.1	
α_g	0.4	

where the ocean is ice covered below $T_{\alpha,l}$ and it is ice free above $T_{\alpha,u}$.

The flux $R_o(T)$ of energy leaving the planet's surface is written with allowance for the CO_2 changes in the atmosphere [24]

$$R_o(T) = B_0 + B_1(T - T_{\mathrm{opt}}),$$

where T_{opt} stands for the temperature, which is optimal for the evolution of vegetation, and B_0 and B_1 are the model parameters estimated in [24].

The coefficient $\beta(T)$ describing the growth rate of vegetation also depends on the optimal temperature T_{opt},

$$\beta(T) = \max\{0, 1 - k(T - T_{\mathrm{opt}})^2\},$$

where k is a constant. The mean death rate of the global vegetation A is determined by the parameter γ entering in the second equation (1). Taking into account the estimates given in Ref. [24] and to demonstrate the main effects of this study, we consider the following range of the death rate: $\gamma \in (0, 0.4)$. All other parameters are listed in Table I.

Let us briefly discuss the main features of deterministic dynamics. System (1) is bistable (see the phase portraits in Fig. 1). For any value of the parameter γ, there is a stable equilibrium $\bar{T}_0 = 242$ K, $\bar{A}_0 = 0$ (black filled circle) corresponding to the snowball case. Along with this "cold" state, the system possesses a "warm" regime in two forms: stable equilibrium for $\gamma > \gamma_H$ [gray filled circle in Fig. 1(a)] and self-oscillations [gray limit cycle in Fig. 1(b)] for $\gamma < \gamma_H$, where $\gamma_H \approx 0.0257$ is the Hopf bifurcation point. Note that the basins of attraction of "cold" and "warm" regimes are separated by the stable manifold (dashed green line) of the saddle point (empty circle). In the bifurcation diagrams in Fig. 2, extrema of system attractors for warm regime are shown in T-γ coordinate plane (a), and A-γ coordinate plane (b).

The limit cycles of system (1) are shown in Fig. 3 for several values of the death rate γ. It should be noted that the amplitude of oscillations for A coordinate essentially changes and attains a maximum at $\gamma \approx 0.02$.

The bifurcation diagrams plotted in Fig. 4 for $\gamma = 0.01$ illustrate that the variations of parameter k also cause some essential changes in the system dynamics. Here, system (1) has
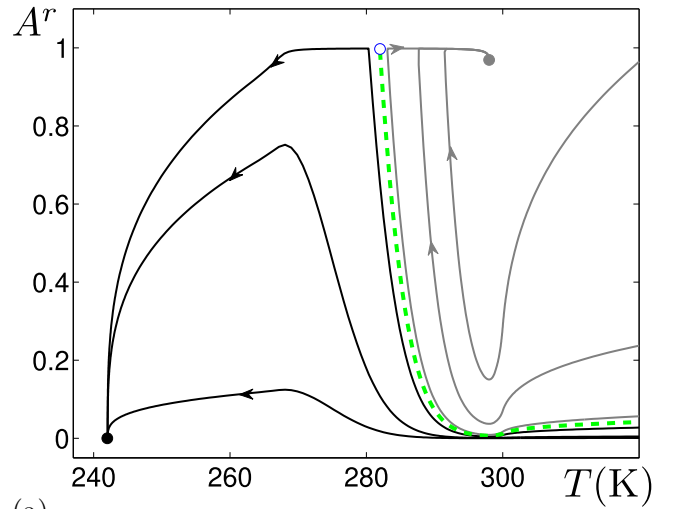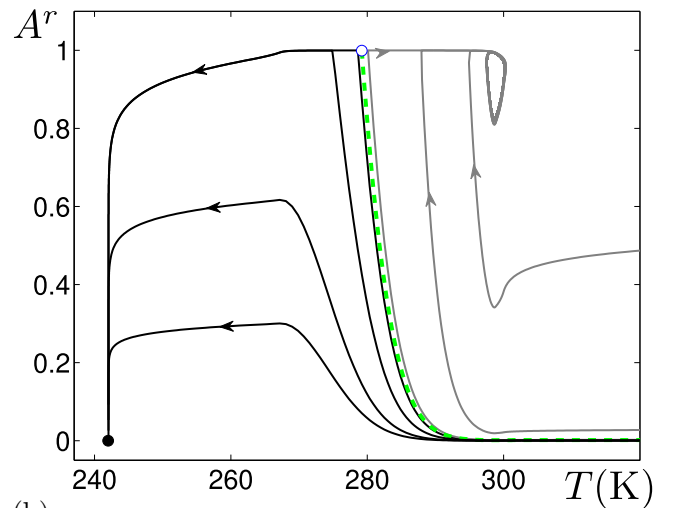
FIG. 1. Phase portrait of system (1) with $k = 0.004$ for (a) $\gamma = 0.1$, (b) $\gamma = 0.02$. To see the details, we use here a nonlinear scaling A^r with $r = \frac{1}{64}$. The separatrix between basins of "cold" and "warm" attractors is shown by the green dashed line.

two Hopf bifurcation points between which self-oscillations exist. In the case of stochastic forcing, the system dynamics changes drastically. How random disturbances of different types influence the system behavior is detailed below.

III. NOISE-INDUCED PHENOMENA

To study some important effects in the evolutionary behavior of the temperature-vegetation model, let us introduce the parametric and additive noises into the second equation of system (1), which model fluctuations in the death rate of vegetation and its growth rate

$$C_T \frac{dT}{dt} = [1 - \alpha(T, A)]Q_0 - R_o(T),$$

$$\frac{dA}{dt} = \beta(T)A(1 - A) - [\gamma + \varepsilon\sigma_1\xi_1(t)]A + \varepsilon\sigma_2\xi_2(t), \quad (2)$$
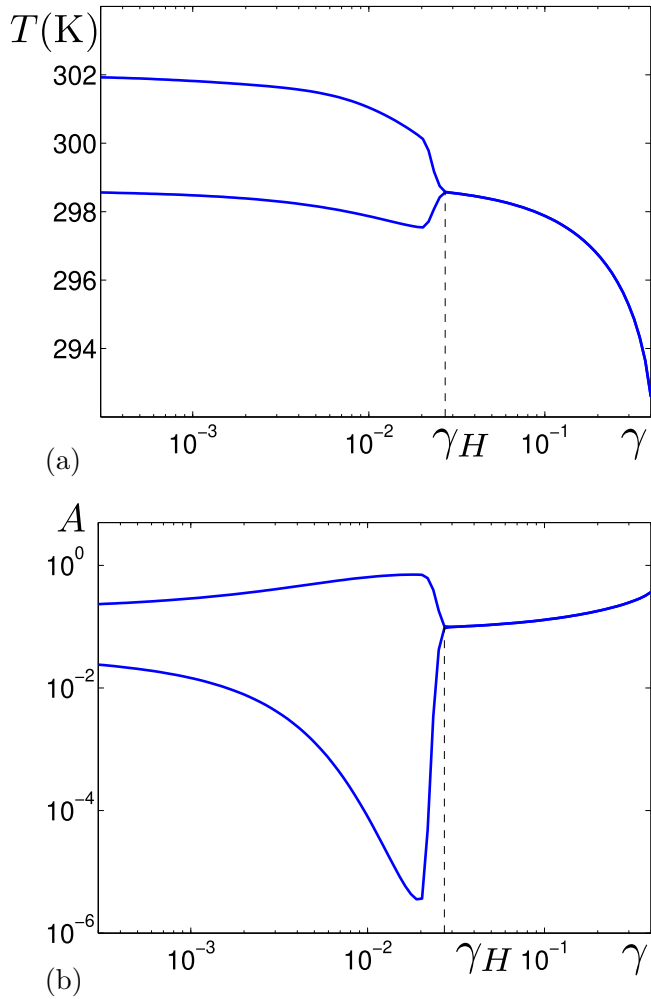
(a)

(b)

FIG. 2. Bifurcation diagram for $k = 0.004$ versus parameter γ.

where $\xi_1(t)$ and $\xi_2(t)$ are the standard uncorrelated white Gaussian noises with properties $\langle \xi_{1,2}(t) \rangle = 0$, $\langle \xi_{1,2}(t)\xi_{1,2}(t + \tau) \rangle = \delta(\tau)$, $\langle \xi_1(t)\xi_2(t + \tau) \rangle = 0$. Parameters ε, $\sigma_{1,2}$ define the noise intensities. The term $\varepsilon\sigma_1\xi_1(t)$ characterizes the random fluctuations of the parameter γ, so that the system is driven by the multiplicative noise. The term $\varepsilon\sigma_2\xi_2(t)$ corresponds to the additive noise.

For numerical simulations of the stochastic system solutions, we use the standard Euler-Maruyama scheme with the time step 10^{-4}. In order to provide the physical sense and keep $A(t) \in [0, 1]$ in the presence of stochastic disturbances, we use the natural truncation: if $A > 1$ then $A = 1$, and if $A < 0$ then $A = 0$.

A. Effects of weak noise

Under weak noise, a random trajectory leaves the deterministic attractor (stable equilibrium or limit cycle) and forms some random distribution localized around it. In Fig. 5(a), the random states (gray dots) of system (2) around the deterministic equilibria (black dots) are plotted for $\sigma_1 = 1$, $\sigma_2 = 0$, and $\varepsilon = 0.02$ for two values of parameter γ: $\gamma = 0.1$ (right) and $\gamma = 0.2$ (left). As can be seen, the random noise of the same intensity results in the different sizes of dispersion. It
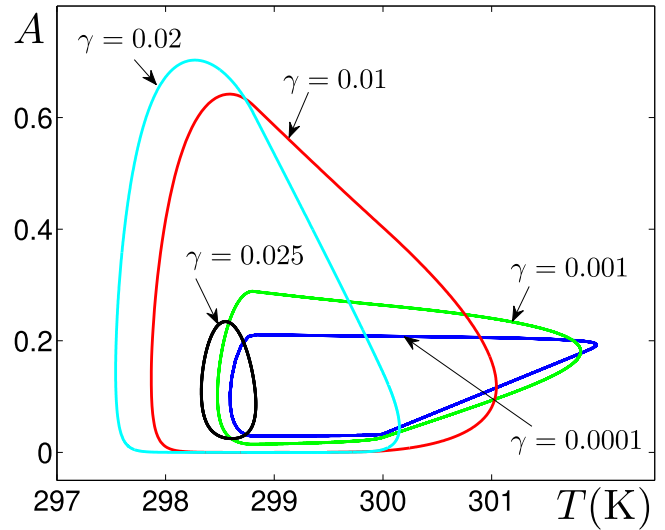

FIG. 3. Deterministic cycles.

can be explained by the difference in stochastic sensitivity of the equilibria for $\gamma = 0.1$ and 0.2. It is significant to note that the random distribution around the equilibrium moves to smaller temperatures with increasing the vegetation death
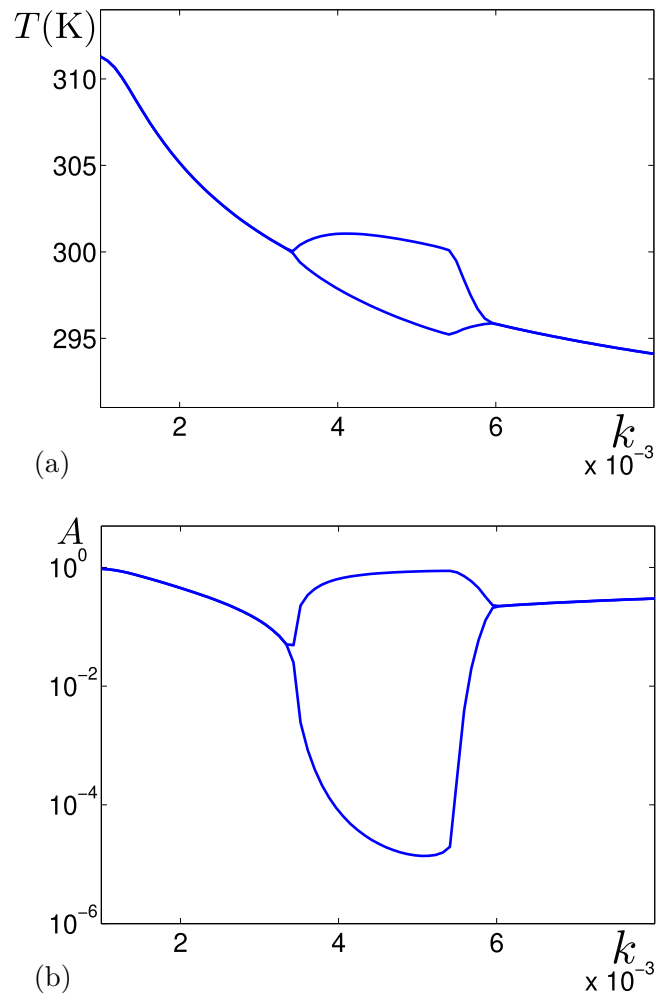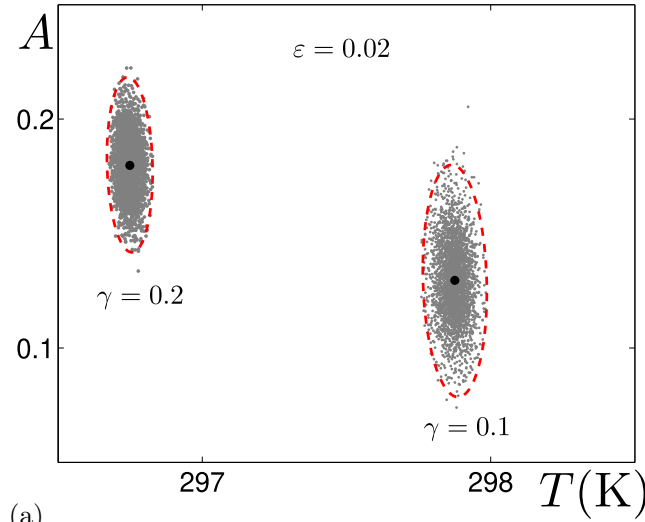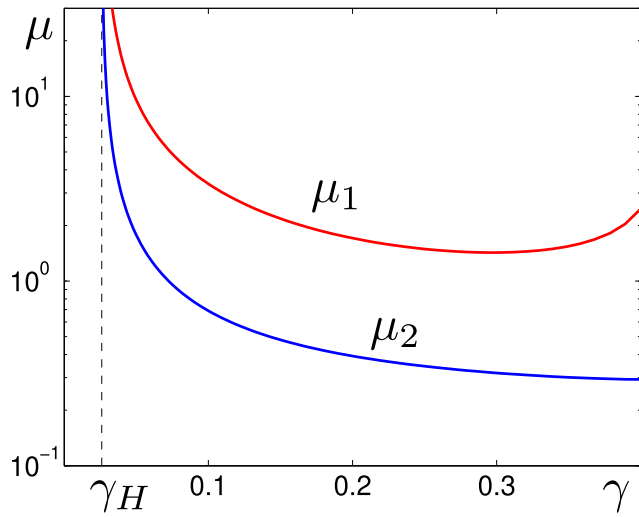

(a)

(b)

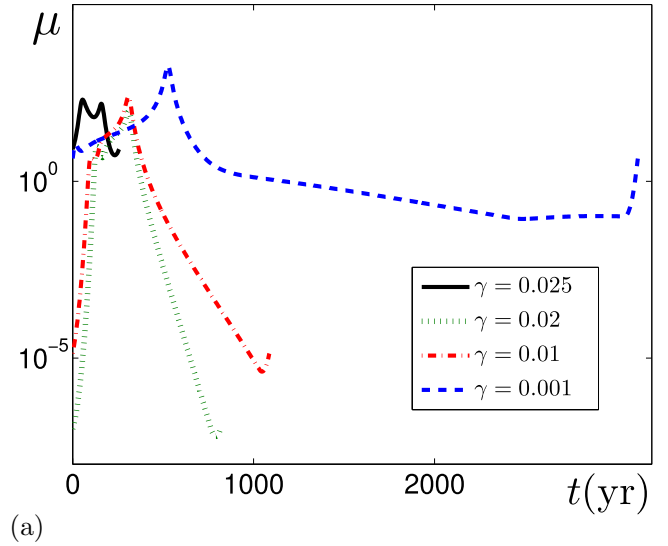FIG. 4. Bifurcation diagram for $\gamma = 0.01$ versus parameter k.

(a)

(b)

FIG. 5. Stochastic system with $\sigma_1 = 1$, $\sigma_2 = 0$: (a) random states and confidence ellipses for $\gamma = 0.1$, $\gamma = 0.2$, and $\varepsilon = 0.02$; (b) eigenvalues $\mu_{1,2}(\gamma)$ of the stochastic sensitivity matrix of equilibria.

(a)

(b)

FIG. 6. Stochastic sensitivity of cycles in system (2) with $\sigma_1 = 1$, $\sigma_2 = 0$: (a) functions $\mu(t)$ for different γ; (b) stochastic sensitivity function (black) shown above the limit cycle (gray) for $\gamma = 0.01$.

rate γ [Fig. 5(a)]. As this takes place, the dispersion of random states decreases. A quantitative analysis of stochastic sensitivity [27,28] of stable equilibria for the system (2) can be carried out as follows (see a theoretical background in the Appendix).
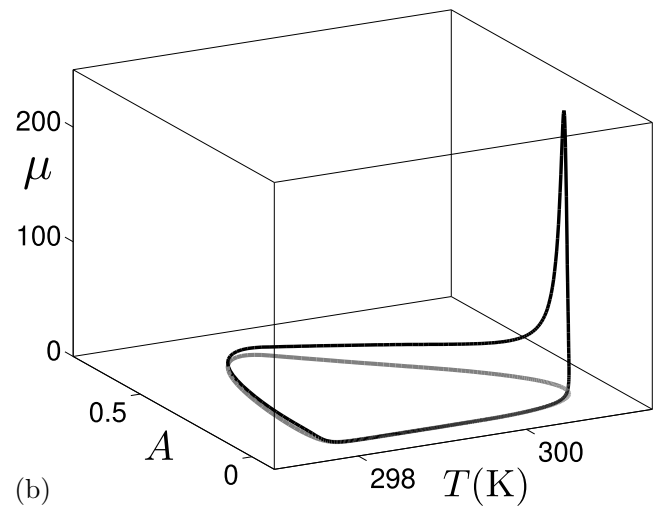
Here, the main characteristic is the stochastic sensitivity matrix W which is a unique solution of the matrix equation (A3), where F is a Jacobi matrix of the deterministic system (1) at the equilibrium point $(\bar{T}, \bar{A})$, and

$$Q = \begin{bmatrix} 0 & 0 \\ 0 & \sigma_1^2 \bar{A}^2 + \sigma_2^2 \end{bmatrix}.$$

Eigenvalues μ_1 and μ_2 of the matrix W are useful scalar characteristics of the noise sensitivity. Eigenvalues μ_1, μ_2 and the corresponding normalized eigenvectors u_1 and u_2 of W determine the size and axes of the confidence ellipse around

$(\bar{T}, \bar{A})$:

$$\frac{x_1^2}{\mu_1} + \frac{x_2^2}{\mu_2} = -2\varepsilon^2 \ln(1 - P),$$

where x_1, x_2 are the coordinates of this ellipse in the basis u_1, u_2 with the point $(\bar{T}, \bar{A})$ as the origin, ε is the noise intensity, and P is the fiducial probability. Here and further, we use the fiducial probability value $P = 0.99$.

Plots of $\mu_1(\gamma)$ and $\mu_2(\gamma)$ for $\sigma_1 = 1$, $\sigma_2 = 0$ are shown in Fig. 5(b). As one can see, the stochastic sensitivity of equilibria essentially depends on γ and tends to infinity as γ approaches the Hopf bifurcation value γ_H.

Using this theory of stochastic sensitivity, we have constructed the confidence ellipses [dashed lines, Fig. 5(a)] for the noise intensity $\varepsilon = 0.02$, $\sigma_1 = 1$, $\sigma_2 = 0$ and two values of the parameter γ. As can be seen, these confidence ellipses are different in size and well agree with the spatial arrangement of random states (gray dots) found by numerical simulations.
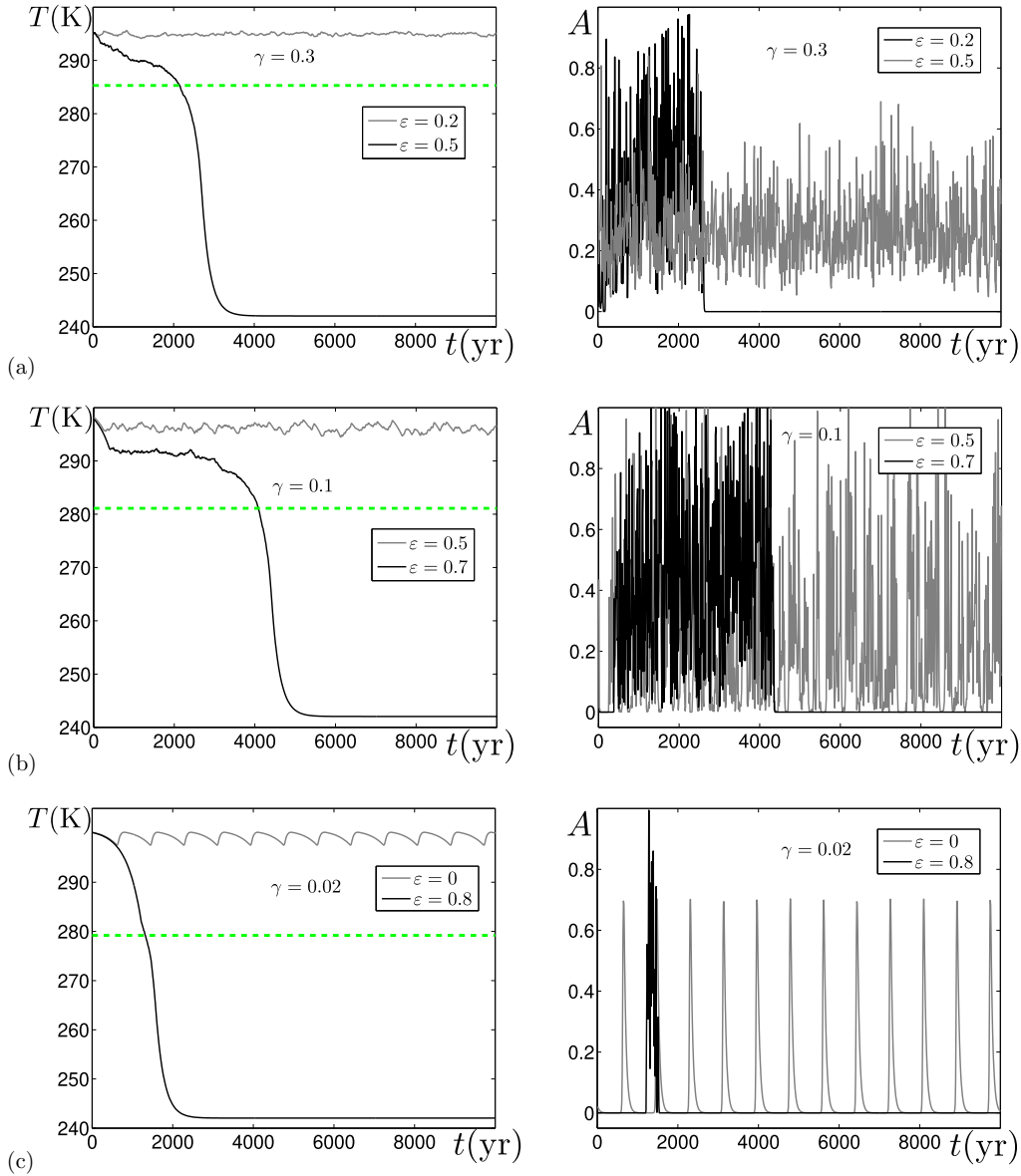
FIG. 7. Multiplicative-noise-induced "freezing" in system (2) with $\sigma_1 = 1$, $\sigma_2 = 0$ and (a) $\gamma = 0.3$, (b) $\gamma = 0.1$, (c) $\gamma = 0.02$. Here the T coordinate of the unstable equilibrium marking the separatrix is shown by the green dashed line.

A dispersion of random states around the stable limit cycle can be also analytically described on the base of the stochastic sensitivity analysis. Let $(\bar{T}(t), \bar{A}(t))$ is a temporal parametrization of the points of the stable limit cycle of system (1) with the period $\bar{t}$. In system (2), the stochastic sensitivity function $\mu(t)$ of this cycle is a unique solution of the boundary value problem (A4) with coefficients $F(t)$ and

$$Q(t) = \begin{bmatrix} 0 & 0 \\ 0 & \sigma_1^2 \bar{A}^2(t) + \sigma_2^2 \end{bmatrix}.$$

Here, $F(t)$ is the Jacobi matrix at the current point $(\bar{T}(t), \bar{A}(t))$ of the cycle, and $p(t) = (p_T(t), p_A(t))^\top$ is a normalized vector that is orthogonal to the cycle at the point $(\bar{T}(t), \bar{A}(t))$.

Plots of $\mu(t)$ for different γ are shown in Fig. 6(a). As can be seen, the function $\mu(t)$ significantly changes along the

cycle. Some details of such a nonuniformity can be seen in Fig. 6(b) for $\gamma = 0.01$.

An important point is that the stochastic system (2) exhibits the nonlocal effects with increasing noise. These effects are essentially different for the cases of multiplicative and additive noises.

B. How a multiplicative noise "freezes" the system

Let us consider how a multiplicative noise affects the system in the absence of the additive noise. To do this, we fix $\sigma_1 = 1$, $\sigma_2 = 0$ and increase the noise intensity ε. In Fig. 7, we show the time series of system (2) starting from the deterministic attractors (equilibria or cycles) for different γ and ε.

For weak noise, the time series exhibit small-amplitude stochastic oscillations near deterministic attractors [see
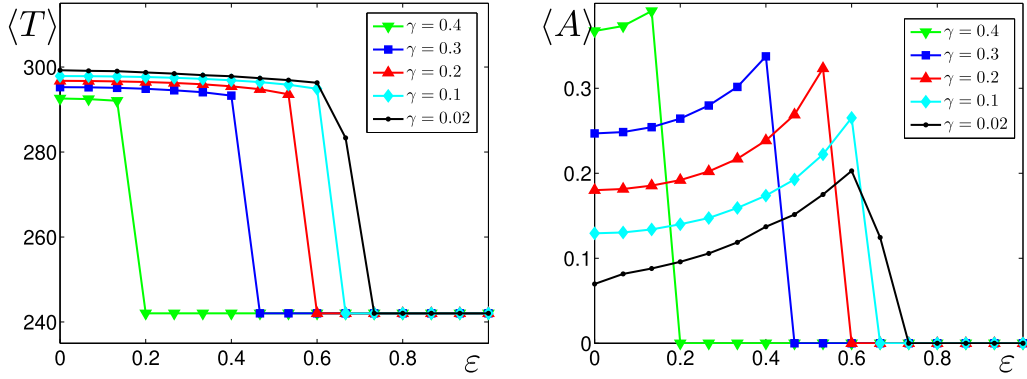
FIG. 8. Multiplicative-noise-induced "freezing" in system (2) with $\sigma_1 = 1$, $\sigma_2 = 0$. The mean values of T and A coordinates are shown in the vertical axes.

Figs. 7(a) and 7(b), gray]. As noise intensity ε exceeds some threshold value, the T coordinate of the solution exhibits a sharp decrease, crosses the separatrix (green dashed line), and shows stabilization to the "cold" equilibrium. The A coordinate vanishes correspondingly [see Figs. 7(a)–7(c), black]. Such a phenomenon can be interpreted as noise-induced freezing with the transformation of the Earth climate to a "snowball" state.

In addition, some details of such a transformation can be seen in Fig. 8 where the mean values $\langle T \rangle$ and $\langle A \rangle$ are shown versus ε for different γ. The sharp falldown of these plots localizes the ε interval corresponding to the onset of the

noise-induced "freezing." As can be seen, with increasing γ, the threshold noise intensity decreases.

C. How an additive noise "warms up" the system

Now, consider how an additive noise affects the system in the absence of multiplicative noise. In stochastic system (2), we fix $\sigma_1 = 0$, $\sigma_2 = 1$ and increase the noise intensity ε. In Fig. 9 (left), we show the time series of T coordinates of system (2) again starting from the deterministic attractors (equilibrium for $\gamma = 0.1$ and cycle for $\gamma = 0.02$) for different ε. In Fig. 9, we plot the stochastic phase trajectories after
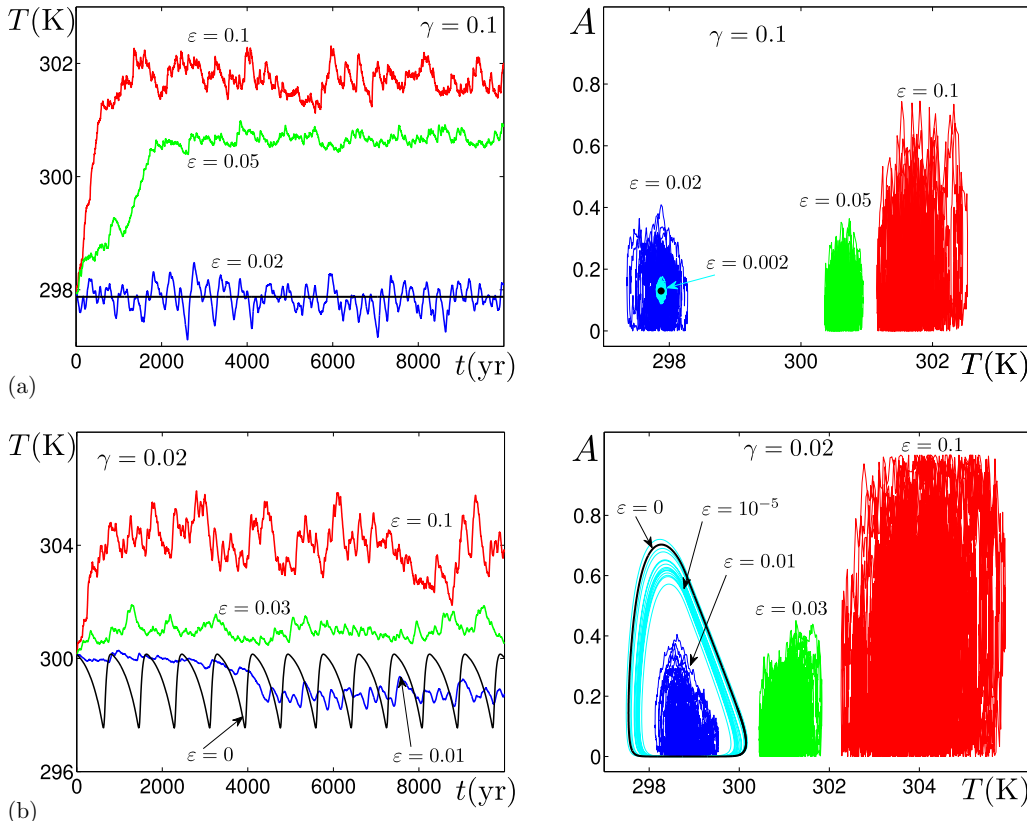

FIG. 9. Additive-noise-induced warming in system (2) with $\sigma_1 = 0$, $\sigma_2 = 1$ and (a) $\gamma = 0.1$, (b) $\gamma = 0.02$.
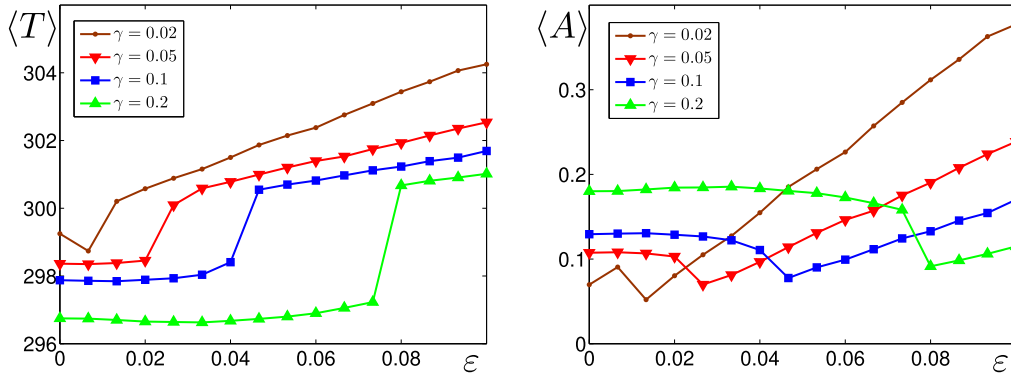
FIG. 10. Additive-noise-induced warming in system (2) with $\sigma_1 = 0$, $\sigma_2 = 1$: mean values of T and A coordinates.

the transient process in the time interval [5×10^4 yr, 6×10^4 yr].

As one can see, for small additive noise, the random trajectories starting from the deterministic attractors fluctuate nearby them. With increasing noise, the T coordinate exhibits a shift to higher temperatures. Such a phenomenon can be interpreted as a noise-induced warming [Fig. 9(a)].

Here, in the case of stable cycles [Fig. 9(b)], an interesting phenomenon is observed: first, the dispersion decreases, the bundle of random trajectories contracts and localizes inside the deterministic cycle (see blue trajectories for $\varepsilon = 10^{-2}$ in Fig. 9, right). Then, the dispersion grows and the bundle of

random trajectories shifts to higher temperatures. It means that the fraction of land A that is covered by the vegetation decreases first and then increases with increasing the additive noise.

Some details of such a transformation are demonstrated in Figs. 10 and 11. In Fig. 10, we show the mean values $\langle T \rangle$ and $\langle A \rangle$ versus ε for different γ. In Fig. 11, the probability density functions $\rho(T)$ and $\rho(A)$ are plotted for $\gamma = 0.1$ and 0.02.

Note that these statistics show the steady growth of the temperature under the increasing intensity of additive noise. As this takes place, the mean value of A also increases in the presence of intervals, where this parameter decreases in a certain range of noise.
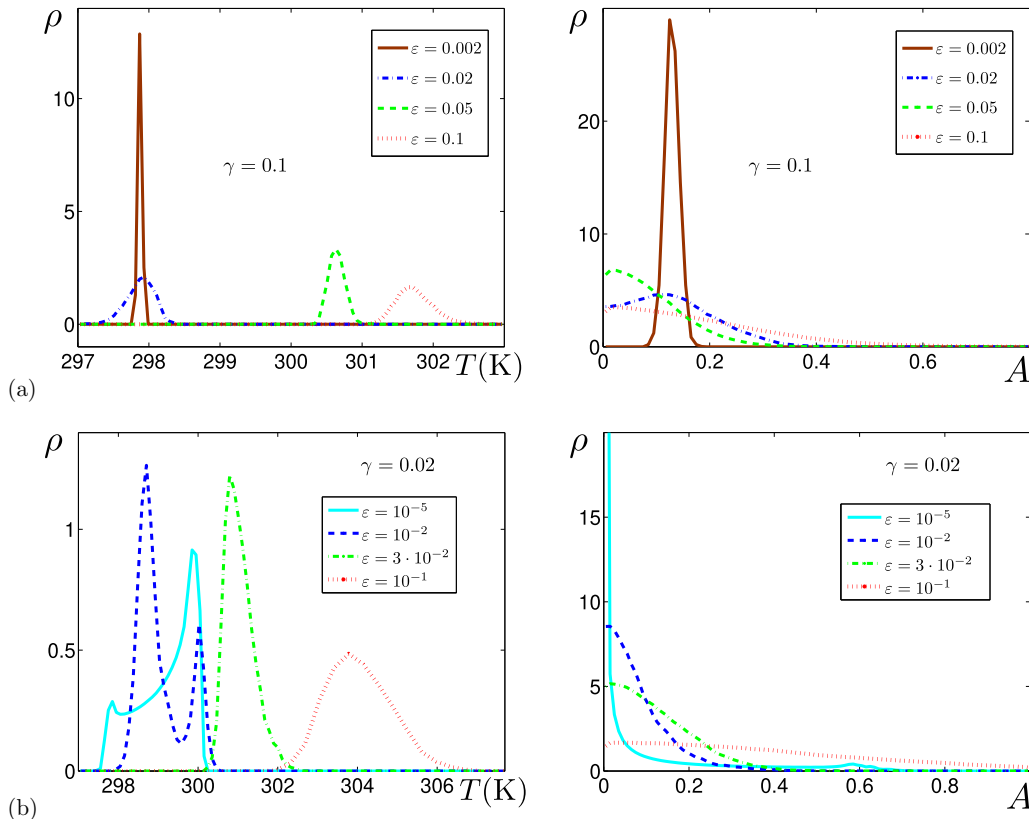

FIG. 11. Additive-noise-induced "warming" in system (2) with $\sigma_1 = 0$, $\sigma_2 = 1$: the probability density functions $\rho(T)$ (left) and $\rho(A)$ (right) for (a) $\gamma = 0.1$, (b) $\gamma = 0.02$.
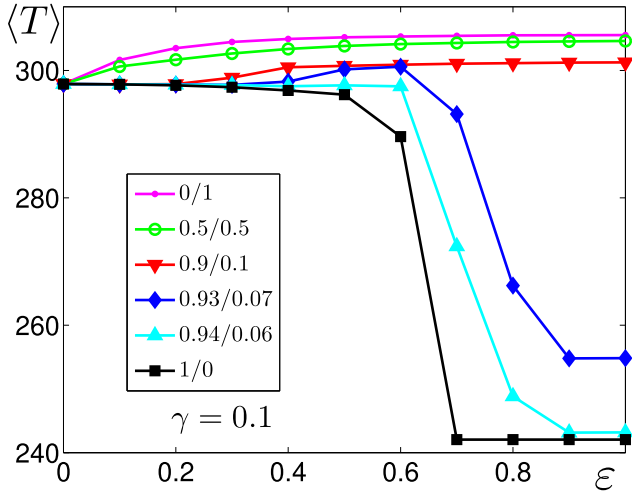
FIG. 12. Corporate effects of multiplicative and additive noises for $\gamma = 0.1$. In the legend, the ratio of σ_1/σ_2 is shown.

D. Corporate effects of multiplicative and additive noises

Consider now a case when the system is driven by both multiplicative and additive noises. In Fig. 12, mean values of the temperature T are plotted versus the noise intensity ε for different weights of multiplicative (σ_1) and additive (σ_2) noises. Here, we use the following normalization: $\sigma_1 + \sigma_2 = 1$.

As can be seen, with the growth of ε, two variants of behavior can be observed in the dependence of weights of these noises. An important point is that an abrupt transition to lower temperatures occurs in the case of multiplicative noise, i.e., in the case of noise in the vegetation death rate.

IV. CONCLUSION

In summary, a simple climate-vegetation model that contains two prognostic variables, the global average temperature and the fraction of land covered by the vegetation, is analyzed with allowance for two different types of noises. The main outcomes of their cooperative occurrence are as follows.

Multiplicative noise. A small multiplicative noise (i.e., the noise in the vegetation death rate) leads to different dispersion of random states at different death rates. In addition, the size of dispersion and average temperature decrease with increasing the death rate. The reason is that the corresponding equilibria of the deterministic model have different stochastic sensitivity. The average temperature and the vegetation fraction undergo a sharp decrease and stabilize at the cold equilibrium with increasing the noise intensity. As this takes place, this transition occurs at smaller noises with increasing the death rate. Thus, the multiplicative noise freezes the climate-vegetation system and transforms it into the snowball state.

Additive noise. A small additive noise builds up the average temperature. As this takes place, the vegetation fraction, which is oscillating within the basin of attraction of a limit cycle or equilibrium at small noises, shifts to higher temperatures. The amplitude of its fluctuations substantially increases with increasing the noise intensity. In general, our statistical analysis shows that the additive noise warms up the

climate-vegetation system, which fluctuates at greater values of T and A.

Cumulative (multiplicative and additive) noise. First of all, a cumulative noise comprises the effects of the multiplicative and additive noises in cases of their corresponding weights. In other words, the multiplicative noise cools down the system and the additive one warms up its dynamics. The ratio of noise weights determining the evolutionary tendency of a climate-vegetation system is studied.

Let us especially emphasize in conclusion that we restrict ourselves by the effects of white Gaussian noises with a wide range of intensities. This type of noise is traditionally used by researchers as a first step in studying the transition from deterministic to stochastic dynamics. Of course, it is of interest to study the impact of colored or Lévy noises. However, to demonstrate the discovered phenomena of stochastic behavior, the use of white noises turned out to be sufficient. The study of colored and Lévy noises represents the subject of future research.

APPENDIX: STOCHASTIC SENSITIVITY FUNCTION

Consider a general nonlinear n-dimensional deterministic system

$$\dot{x} = f(x) \qquad (A1)$$

with an exponentially stable attractor Γ in the domain D. To study an influence of random disturbances, we use the following system of stochastic differential equations:

$$\dot{x} = f(x) + \varepsilon\sigma(x)\xi(t), \qquad (A2)$$

where $\sigma(x)$ is an $n \times m$ matrix function, $\xi(t)$ is an m-dimensional uncorrelated white Gaussian noise with parameters $\langle \xi(t) \rangle = 0$, $\langle \xi(t)\xi^\top(\tau) \rangle = \delta(t - \tau)I$, and ε is the noise intensity.

In the presence of noise, trajectories of system (A2) form some random distribution around the deterministic attractor Γ. For weak noise, the stationary density $\rho(x, \varepsilon)$ has the asymptotics [29] based on the quasipotential $v(x) = -\lim_{\varepsilon \to 0} \varepsilon^2 \log \rho(x, \varepsilon)$. The quasipotential is governed by the Hamilton-Jacobi equation

$$\left(f(x), \frac{\partial v}{\partial x} \right) + \frac{1}{2}\left(\frac{\partial v}{\partial x}, \sigma(x)\sigma^\top(x)\frac{\partial v}{\partial x} \right) = 0$$

with conditions $v|_\Gamma = 0$, $v|_{D\setminus\Gamma} > 0$. In the vicinity of deterministic attractors, quadratic approximations of the quasipotential can be used [30].

1. Stochastic sensitivity of the equilibrium

Let the deterministic system (A1) has an exponentially stable equilibrium $\bar{x}$. In the vicinity of $\bar{x}$, the quadratic approximation of the quasipotential is written as $v(x) \approx \frac{1}{2}(x - \bar{x}, W^{-1}(x - \bar{x}))$. Here, the positive definite $n \times n$ matrix W is the *stochastic sensitivity matrix of the equilibrium* [31]. This

matrix is a unique solution of the equation

$$FW + WF^\top = -Q,$$
$$F = \frac{\partial f}{\partial x}(\bar{x}), \quad Q = GG^\top, \quad G = \sigma(\bar{x}). \quad \text{(A3)}$$

Using the stochastic sensitivity matrix W, one can find the asymptotics of the stationary distribution $\rho(x, \varepsilon)$ in the Gaussian form

$$\rho(x, \varepsilon) \approx K \exp\left(-\frac{(x - \bar{x}, W^{-1}(x - \bar{x}))}{2\varepsilon^2}\right).$$

The stochastic sensitivity matrix characterizes a form and size of the stationary distribution of random states of system (A2) around the deterministic equilibrium $\bar{x}$.

2. Stochastic sensitivity of the cycle

Let the deterministic system (A1) has an exponentially stable limit cycle $\bar{x}(t)$ corresponding to the T-periodic solution $x = \bar{x}(t)$. Denote by Π_t a hyperplane that is orthogonal to the cycle at the point $\bar{x}(t)$ ($0 \leqslant t < T$). For the Poincare section Π_t in the neighborhood of the point $\bar{x}(t)$, one can write the quadratic approximation of the quasipotential: $v(x) \approx \frac{1}{2}(x - \bar{x}(t), W^+(t)[x - \bar{x}(t)])$ (the sign "+" means a pseudoinversion). A corresponding Gaussian approximation of the

stationary probabilistic distribution can be written as

$$\rho_t(x, \varepsilon) \approx K \exp\left(-\frac{[x - \bar{x}(t)]^\top W^+(t)[x - \bar{x}(t)]}{2\varepsilon^2}\right).$$

The matrix $W(t)$ is the *stochastic sensitivity matrix of the cycle* [27,32]. This matrix is a unique solution of the boundary problem

$$\dot{W} = F(t)W + WF^\top(t) + P(t)Q(t)P(t),$$
$$W(0) = W(T), \quad W(t)r(t) \equiv 0.$$

Here, $F(t) = \frac{\partial f}{\partial x}(\bar{x}(t))$, $Q(t) = \sigma(\bar{x}(t))\sigma^\top(\bar{x}(t))$, $r(t) = f(\bar{x}(t))$, and $P(t) = I - r(t)r^\top(t)/(r^\top(t)r(t))$.

In the two-dimensional case, the stochastic sensitivity of the cycle is defined by a scalar T-periodic function $\mu(t)$: $W(t) = \mu(t)p(t)p^\top(t)$. Here, $p(t)$ is a normalized vector that is orthogonal to the cycle at the point $\bar{x}(t)$. The function $\mu(t)$ is a unique solution of the boundary value problem

$$\dot{\mu} = a(t)\mu + b(t), \quad \mu(0) = \mu(T) \quad \text{(A4)}$$

with coefficients $a(t) = p^\top(t)[F^\top(t) + F(t)]p(t)$, $b(t) = p^\top(t)Q(t)p(t)$. The function $\mu(t)$ has an explicit representation $\mu(t) = u(t)[c + s(t)]$, where

$$u(t) = \exp\left(\int_0^t a(\tau)d\tau\right), \quad s(t) = \int_0^t \frac{b(\tau)}{u(\tau)}d\tau,$$
$$c = \frac{u(T)s(T)}{1 - u(T)}.$$

[1] F. Woodward, *Climate and Plant Distribution* (Cambridge University Press, Cambridge, 1987).

[2] D. Zemp, C.-F. Schleussner, H. Barbosa, M. Hirota, V. Montade, G. Sampaio, A. Staal, L. Erlandsson, and A. Rammig, Nat. Commun. **8**, 14681 (2017).

[3] G. Duveiller, J. Hooker, and A. Cescatti, Nat. Commun. **9**, 679 (2018).

[4] M. Claussen, S. Bathiany, V. Brovkin, and T. Kleinen, Nat. Geosci. **6**, 954 (2013).

[5] U. Port and M. Claussen, Clim. Past **11**, 1563 (2015).

[6] G. Ferraz, J. Nichols, J. Hines, P. Stouffer, J. R. O. Bierregaard, and T. Lovejoy, Science **315**, 238 (2007).

[7] A. Pitman and R. Lorenz, Environ. Res. Lett. **11**, 094025 (2016).

[8] K. Ikazaki, Soil Sci. Plant Nutr. **61**, 372 (2015).

[9] G. Wang and E. Eltahir, Geophys. Res. Lett. **27**, 795 (2000).

[10] B. Saltzman, *Dynamical Paleoclimatology: Generalised Theory of Global Climate Change* (Academic, New York, 2002).

[11] M. Crucifix, Philos. Trans. R. Soc. A **370**, 1140 (2012).

[12] D. V. Alexandrov, I. A. Bashkirtseva, and L. B. Ryashko, Phys. D (Amsterdam) **343**, 28 (2017).

[13] Z. Liu, Y. Wang, R. Gallimore, F. Gasse, T. Johnson, P. deMenocal, J. Adkins, M. Notaro, I. Prentice, J. Kutzbach, R. Jacob, P. Behling, L. Wang, and E. Ong, Quat. Sci. Rev. **26**, 1818 (2007).

[14] D. V. Alexandrov, I. A. Bashkirtseva, and L. B. Ryashko, Tellus **66**, 23454 (2014).

[15] W. Horsthemke and R. Lefever, *Noise-Induced Transitions* (Springer, Berlin, 1984).

[16] B. Lindner, J. García-Ojalvo, A. Neiman, and L. Schimansky-Geier, Phys. Rep. **392**, 321 (2004).

[17] V. Anishchenko, V. Astakhov, A. Neiman, T. Vadivasova, and L. Schimansky-Geier, *Nonlinear Dynamics of Chaotic and Stochastic Systems. Tutorial and Modern Development* (Springer, Berlin, 2007).

[18] M. D. McDonnell, N. G. Stocks, C. E. M. Pearce, and D. Abbott, *Stochastic Resonance: From Suprathreshold Stochastic Resonance to Stochastic Signal Quantization* (Cambridge University Press, Cambridge, 2008), p. 446.

[19] A. S. Pikovsky and J. Kurths, Phys. Rev. Lett. **78**, 775 (1997).

[20] D. V. Alexandrov, I. A. Bashkirtseva, and L. B. Ryashko, Phys. D (Amsterdam) **399**, 153 (2019).

[21] J. B. Gao, S. K. Hwang, and J. M. Liu, Phys. Rev. Lett. **82**, 1132 (1999).

[22] I. Bashkirtseva and L. Ryashko, Phys. Lett. A **380**, 3359 (2016).

[23] V. Lucarini, Phys. Rev. E **100**, 062124 (2019).

[24] J. Rombouts and M. Ghil, Nonlin. Process. Geophys. **22**, 275 (2015).

[25] W. Sellers, J. Appl. Meteorol. **8**, 392 (1969).

[26] M. Ghil, J. Atmos. Sci. **33**, 3 (1976).

[27] I. Bashkirtseva, L. Ryashko, and E. Slepukhina, Fluctuation Noise Lett. **13**, 1450004 (2014).

[28] I. Bashkirtseva, A. B. Neiman, and L. Ryashko, Phys. Rev. E **91**, 052920 (2015).

[29] M. I. Freidlin and A. D. Wentzell, *Random Perturbations of Dynamical Systems* (Springer, New York, 1984).

[30] G. Mil'shtein and L. Ryashko, J. Appl. Math. Mech. **59**, 47 (1995).

[31] I. Bashkirtseva and L. Ryashko, Phys. Rev. E **83**, 061109 (2011).

[32] I. Bashkirtseva and L. Ryashko, Math. Comput. Simulation **66**, 55 (2004).